

Compact Planar Quad-Band Bandpass Filter for Application in GPS, WLAN, WiMAX and 5G WiFi

Mojtaba Mirzaei and Mohammad A. Honarvar*

Abstract—In this paper, a novel compact second-order quad-band bandpass filter (BPF) is applied based on a novel quintuple-mode stub-loaded trigonal ring resonator. Resonant characteristics are extracted by even- and odd-mode method. Designing procedure of resonant frequencies has also been presented. The last two resonant modes are utilized to cover a wide bandwidth for 5G WiFi application. The rest of other three resonant modes are used to form three passbands for GPS, WLAN and WiMAX applications. According to pseudo-interdigital structure four transmission zeros are generated among passbands to improve the band to band rejection and enhance the frequency selectivity. The measurement results agree well with the EM simulation ones.

1. INTRODUCTION

With the increasing demand for multi-service wireless systems, microwave components that support multi-band operations have received much attention. As an essential component of the multi-band transceivers, multi-band bandpass filters (BPFs) designed with compact size, high selectivity, and practical operation bands have been extensively investigated to enhance the system functionality. However, previous works have focused mostly on dual- and tri-band BPFs.

A popular approach for designing dual- and tri-band BPFs is the utilization of multi-mode resonators (MMRs) [1–5]. In [1], dual-band BPFs are presented using dual-mode stub-loaded stepped impedance resonators. Resonant frequencies are controlled with stub dimensions. A single short-ended dual-mode resonator is used to present a dual-band BPF [2]. In [3], a tri-band BPF based on two sets of short stub-loaded stepped impedance resonators and a pair of embedded stepped impedance resonators is realized. In [4], a tri-band BPF is presented using stub-loaded short-ended resonator. A quad-mode resonator is used to create desirable bandwidths of a dual band BPF [5].

Quad-band bandpass filters have thrived in recent years [6–13]. In [6], a quad-band BPF is achieved based on splitting two passbands of a dual-band BPF by transmission zeros (TZs). This method is not applicable when there is a great distance between pass bands. In [7, 8], quad-band BPFs are proposed using multi-layered structures composed of microstrip and defected ground structure resonators. Two sets of dual-mode resonators are applied to realize a quad-band BPF in [9]. However, the combination of resonators increases the circuit size. Recently, an attractive method utilizing a single multi-mode resonator has been applied to develop compact multi-band BPFs. In [10–12], quad-mode resonators that resonate at the four desired frequencies are used to present quad-band BPFs. In [13], a single stepped-impedance ring loaded resonator with eight resonant modes is utilized to create four passbands of a bandpass filter.

Although single multi-mode BPFs occupy less circuit size, it will be hard to adjust the resonant modes of the MMR for filters with many passbands. In addition, the operating band of 5G WiFi

Received 23 September 2016, Accepted 20 October 2016, Scheduled 4 November 2016

* Corresponding author: Mohammad Amin Honarvar (Amin.Honarvar@pel.iaun.ac.ir).

The authors are with Department of Electrical Engineering, Najafabad Branch, Islamic Azad University, Najafabad, Iran.

(5.15 GHz–5.85 GHz) has a wide bandwidth and more resonant frequencies are required to cover it. Thus, limited multi-band BPFs with 5G WiFi application have been reported until now [14].

In this paper, a quintuple-mode stub-loaded trigonal ring resonator (SLTRR) is applied to design a compact second-order quad-band bandpass filter (BPF). Even- and odd-mode method is applied to extract SLTRR resonant characteristics. The last two frequency modes are utilized to form a passband that covers the 5G WiFi operating band. The rest of the three modes are centered at 1.55 GHz, 2.44 GHz, and 3.48 GHz for GPS, WLAN, and WiMAX applications, respectively. Based on pseudo-interdigital structure four transmission zeros are generated around the passbands to improve the selectivity. The measured results show good agreement with the simulation results.

2. QUINTUPLE-MODE SLTRR ANALYSIS

Figure 1(a) shows the basic prototype of the proposed quintuple-mode SLTRR. It consists of a trigonal ring loaded by a short-circuit stub and two open-circuit arms that added to both sides of the trigonal ring. Two open-circuit arms and the base of trigonal ring act as a half-wavelength resonator. The physical dimension parameters of the SLTRR are indicated by the line lengths of L_1 , L_2 , L_3 , L_4 and widths of W_1 , W_2 , W_3 , and W_4 . Due to the symmetrical structure of the resonator, even- and odd-mode method can be applied to extract resonant characteristics. The even- and odd-mode equivalent circuits are shown in Figures 1(b) and (c), respectively.

Where θ_1 , θ_2 , θ_3 and θ_4 are the electrical lengths and Y_1 , Y_2 , Y_3 and Y_4 are the characteristic admittances of the sections. Based on microwave networks knowledge from [15], the input admittance of a transmission line can be expressed as:

$$Y_{in} = Y_0 \frac{Y_L + jY_0 \tan(\theta)}{Y_0 + jY_L \tan(\theta)} \quad (1)$$

where Y_L is load admittance. Using (1), and according to SLTRR equivalent circuits, the input admittance of the even- and odd-modes are defined as:

$$Y_{in,even} = jY_0 \frac{\tan(\theta_1) - \cot(\theta_2 + \theta_4) + \tan(\theta_3)}{1 + \cot(\theta_2 + \theta_4) \tan(\theta_1) - \tan(\theta_3) \tan(\theta_1)} \quad (2)$$

$$Y_{in,odd} = jY_0 \frac{\tan(\theta_1) - \cot(\theta_2) - \cot(\theta_3)}{1 + \cot(\theta_2) \tan(\theta_1) - \cot(\theta_3) \tan(\theta_1)} \quad (3)$$

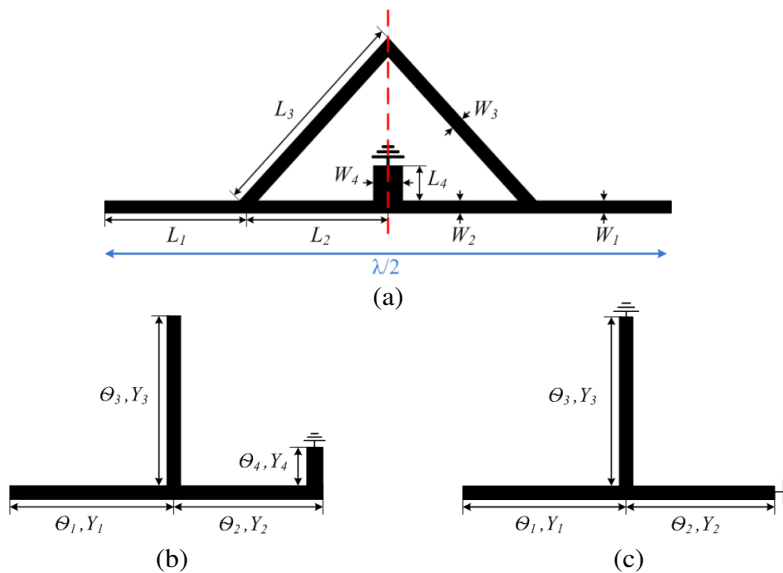


Figure 1. Prototype and equivalent circuit of SLTRR: (a) prototype, (b) even-mode equivalent circuit and (c) odd-mode equivalent circuit.

where $Y_1 = Y_2 = Y_3 = Y_4 = Y_0$ are employed for simplicity. The resonance conditions for the even- and odd-modes are derived from $Y_{in,even} = 0$ and $Y_{in,odd} = 0$ as:

$$\tan(\theta_1) - \cot(\theta_2 + \theta_4) + \tan(\theta_3) = 0 \quad (4)$$

$$\tan(\theta_1) - \cot(\theta_2) - \cot(\theta_3) = 0 \quad (5)$$

Since, two open-circuit arms and the base of trigonal ring form a half-wavelength resonator at the designing frequency of f_0 , it can be considered $\theta_1 = 90^\circ - \theta_2$. Also, because the electrical length of a transmission line is different at different frequencies, the resonance conditions can be rewritten as:

$$\tan\left(\frac{f_{em}}{f_0}(90^\circ - \theta_2)\right) - \cot\left(\frac{f_{em}}{f_0}(\theta_2 + \theta_4)\right) + \tan\left(\frac{f_{em}}{f_0}(\theta_3)\right) = 0, \quad m = 1, 2, 3 \quad (6)$$

$$\tan\left(\frac{f_{on}}{f_0}(90^\circ - \theta_2)\right) - \cot\left(\frac{f_{on}}{f_0}(\theta_2)\right) - \cot\left(\frac{f_{on}}{f_0}(\theta_3)\right) = 0, \quad n = 1, 2 \quad (7)$$

After several times to solve Equation (6), the first three normalized even-mode frequencies $\frac{f_{e1}}{f_0}$, $\frac{f_{e2}}{f_0}$, and $\frac{f_{e3}}{f_0}$ can be obtained for each specific value of θ_2 , θ_3 , and θ_4 . Similarly, for each specific θ_2 and θ_3 , the first two normalized odd-mode frequencies of $\frac{f_{o1}}{f_0}$ and $\frac{f_{o2}}{f_0}$ can be derived from (7). Figures 2(a) and 2(b) illustrate the variation of normalized even- and odd-mode resonant frequencies against different values of θ_2 , θ_3 and fixed condition of $\theta_4 = 5^\circ$ (the efficiency of the short-circuit stub is studied later).

It can be observed that all the normalized even- and odd-mode resonant frequencies decrease as θ_3 increases from 40° to 80° . While as θ_2 increases from 10° to 80° normalized even- and odd-mode resonant frequencies change irregularly. Due to the different variations of normalized frequencies, it can be concluded that the proposed quintuple-mode SLTRR can be used to design different frequency responses.

In this paper, even- and odd-mode resonant frequencies should be adjusted at $f_{e1} = 1.55$ GHz, $f_{o1} = 2.4$ GHz, $f_{e2} = 3.5$ GHz, $f_{o2} = 5.25$ GHz, and $f_{e3} = 5.75$ GHz. After selecting appropriate values for electrical lengths of the SLTRR and the designing frequency of f_0 , even and odd resonant modes can be located at desired frequencies. Figure 3 plots the simulated EM frequency response of the proposed SLTRR for the selected values of $\theta_2 = 37^\circ$, $\theta_3 = 60^\circ$ and $\theta_4 = 5^\circ$ from Figure 2 (denoted by the dashed lines) and $f_0 = 2.2$ GHz. The physical dimensions of the SRLR can be acquired by using the ADS LineCalc tool. Five even and odd resonant modes can be observed at $f_{e1} = 1.63$ GHz, $f_{o1} = 2.44$ GHz, $f_{e2} = 3.45$ GHz, $f_{o2} = 5.25$ GHz, and $f_{e3} = 6.26$ GHz. It is known that the first four resonant modes are located near the desired frequencies, but f_{e3} is far from 5.75 GHz.

As mentioned before, to cover the wide bandwidth of 5G WiFi band (5.15 GHz–5.85 GHz), it needs to have more than one resonant frequencies. Thus, the last two frequency modes can be used to cover it. To accomplish this, the resonant frequencies of the third even-mode (f_{e3}) must shift to about 5.75 GHz frequency ranges. Referring to Figure 1(c), it is obvious that the short-circuit stub dimensions (L_4 , W_4) have no effects on the two odd resonant modes. Thus, the resonant frequencies of the three even-modes can be controlled by changing the short-circuit stub dimensions.

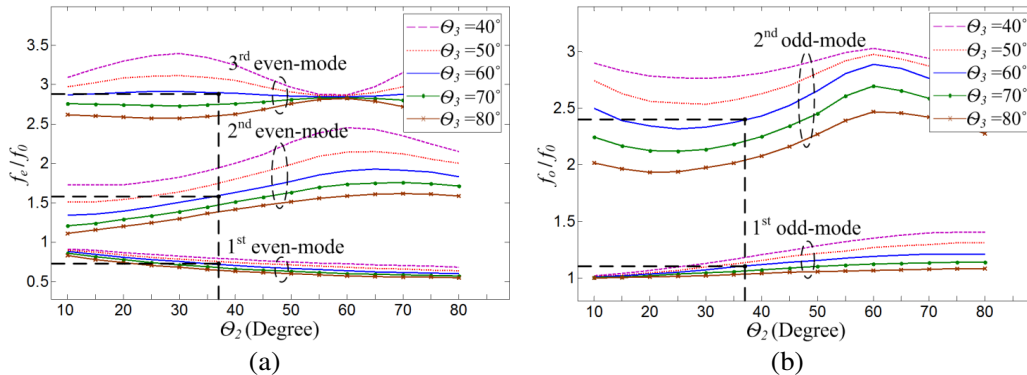


Figure 2. Variation of (a) $\frac{f_e}{f_0}$ and (b) $\frac{f_o}{f_0}$ against different values of θ_2 and θ_3 ($\theta_4 = 5^\circ$ is fixed).

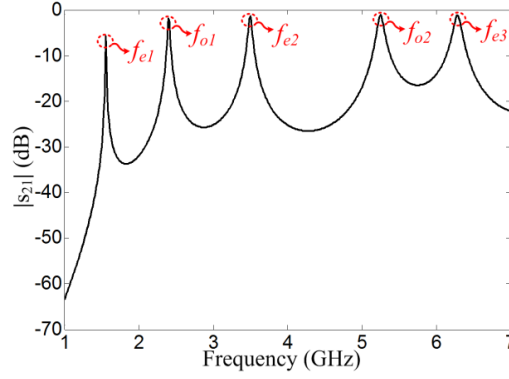


Figure 3. Simulated $|S_{21}|$ of proposed quintuple-mode SLTRR.

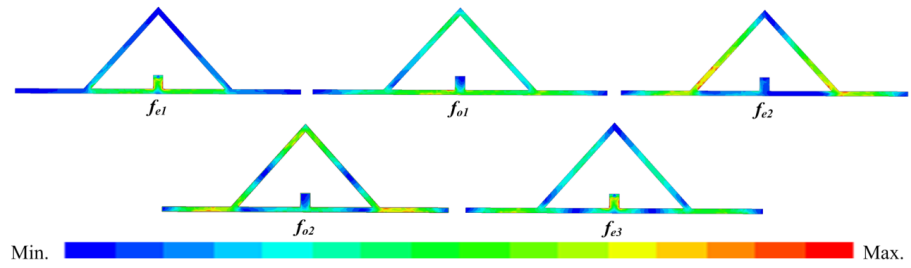


Figure 4. Simulated current density distribution of SLTRR.

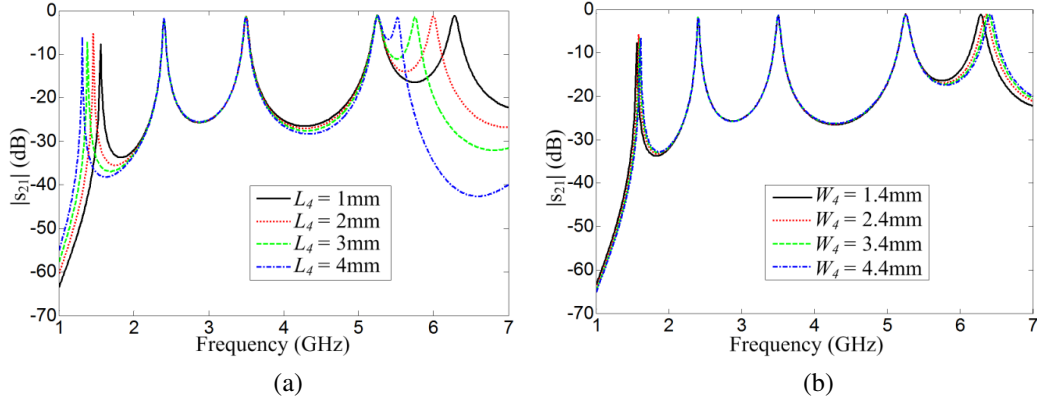


Figure 5. Simulated $|S_{21}|$ of SLTRR for varying: (a) L_4 and (b) W_4 .

Figure 4 shows the simulated current density distribution of the SLTRR at resonant frequencies. It can be seen that only for the first and third even resonant frequencies, current is concentrated on the short-circuit stub. Therefore, by changing the length and width of the short-circuit stub, resonant frequencies of the first and the third even-mode can be controlled. Figures 5(a) and 5(b) depict the variation of the quintuple-mode SLTRR resonant frequencies against different values of W_4 and L_4 . It can be observed that the first and the third even resonant frequencies decrease as L_4 increases and they increase as W_4 increases, while the other three resonant frequencies are approximately fixed.

Figure 6 shows the final structure of the proposed quintuple-mode SLTRR. To reduce the circuit size and fill the blank areas, the trigonal ring sides are folded inwards. Also, because the phase velocity of folded line is a little different than straight line, the resonant modes can be adjusted easier at desired frequencies. In this structure, by choosing $L_4 = 4.6$ mm and $W_4 = 4.4$ mm, resonant frequencies of the first and the third even-mode are shifted to 1.56 GHz and 5.80 GHz, respectively. With the physical

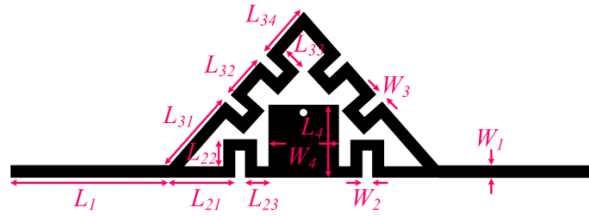


Figure 6. Final structure of proposed quintuple-mode SLTRR.

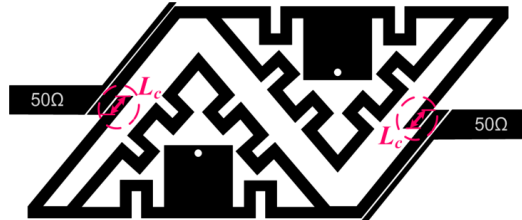


Figure 7. Configuration of designed quad-band BPF.

dimensions of $L_1 = 10.3$, $L_{21} = 3.8$, $L_{22} = 1.7$, $L_{23} = 1.5$, $L_{31} = 5.4$, $L_{32} = 2.75$, $L_{33} = 1.52$, $L_{34} = 3.6$, $W_1 = 0.7$, $W_2 = 0.7$, and $W_3 = 0.6$ (all in millimeters), the other three resonant frequencies are adjusted at 2.42 GHz, 3.51 GHz, and 5.24 GHz.

3. QUAD-BAND BPF DESIGN

Based on the presented quintuple-mode SLTRR, a new second-order quad-band BPF is designed for GPS, WLAN, WiMAX, and 5G WiFi applications. Figure 7 depicts the configuration of quad-band BPF. Two uniform SLTRRs are coupled by pseudo-interdigital structure [16], that also miniaturizes the circuit size and creates the required bandwidth of each passbands. Because of multi-paths propagation mode configuration of the pseudo-interdigital structure, four transmission zeros are generated to achieve good isolation between passbands and improve the selectivity.

The created passbands by two last resonant modes of the SLTRRs are joined together to form a passband that cover the bandwidth of 5G WiFi band. Two coupling paths between open-circuit arms that indicated in Figure 7 are used to achieve suitable bandwidth of four passbands. Figure 8 illustrates the simulated $|S_{11}|$ against three values of $L_c = 0.5$ mm, $L_c = 1.1$ mm, and $L_c = 1.4$ mm and fixed coupling gap (0.15 mm) between lines. It can be observed that the bandwidths of the four passbands increase as L_c increases. However, if L_c gets too big or too small, the minimum magnitude return losses will less than 10 dB.

Therefore, by choosing the appropriate value of $L_c = 1.1$ mm, simulated passbands of the designed quad-mode BPF are centered at 1.55 GHz, 2.44 GHz, 3.48 GHz and 5.49 GHz. The 3 dB bandwidths of each passbands are 4.51% (1.52 GHz–1.59 GHz), 6.55% (2.37 GHz–2.53 GHz), 8.91% (3.34 GHz–3.65 GHz), and 13.66% (5.12 GHz–5.86 GHz), which completely cover GPS, WLAN, WiMAX, and 5G WiFi applications respectively. The minimum simulated insertion losses at the center frequencies are 1.7 dB, 0.96 dB, 0.62 dB, and 0.92 dB and the simulated return losses are better than 13.5 dB, 16.7 dB, 13.9 dB, and 14.1 dB for each passbands.

4. EXPERIMENTAL RESULTS

Finally, the proposed quad-band BPF is fabricated on a Rogers Ro 4003 substrate with dielectric constant of 3.55, thickness of 0.81 mm, and loss tangent of 0.0027. The overall circuit size is 31 mm × 13.3 mm or $0.24\lambda_g \times 0.10\lambda_g$ (λ_g is the guided wavelength at the center frequency of the first passband). Figure 9 shows the simulated and measured frequency responses of the fabricated filter and its photograph. The four measured passbands are centered at 1.55 GHz (GPS), 2.46 GHz (WLAN),

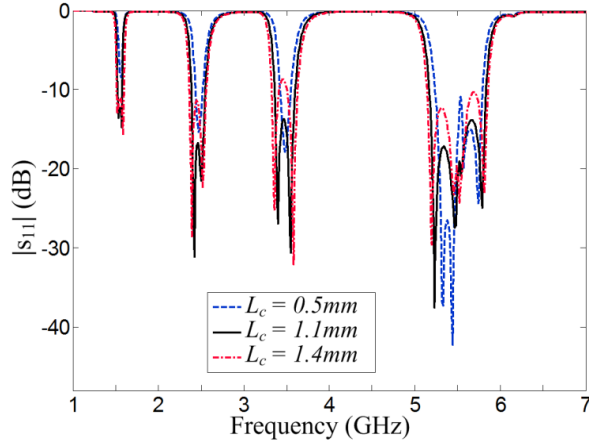


Figure 8. Simulated $|S_{11}|$ of designed quad-band BPF for varying L_c .

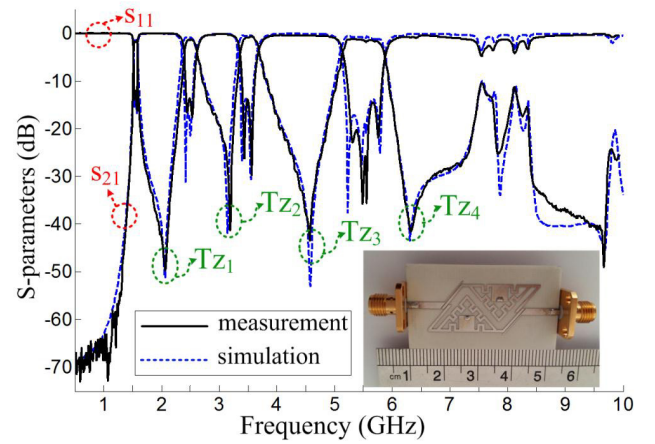


Figure 9. Simulated and measured S -parameters of fabricated quad-band BPF.

3.52 GHz (WiMAX), and 5.51 GHz (5G WiFi) with the 3 dB bandwidth of 4.06%, 5.08%, 7.95%, and 12.36%. The measured insertion losses at the center frequency of each passbands are 1.95 dB, 1.4 dB, 0.9 dB, and 1.55 dB, and the measured return losses are better than 12.2 dB, 13.64 dB, 13.98 dB, and 14.5 dB, respectively. The measured results show a fairly good agreement with the simulated result and the discrepancy is attributed to the unexpected tolerance of fabrication and implementation.

Due to multi-paths propagation mode configuration of the pseudo-interdigital coupling structure, four transmission zeros at 2.06 GHz, 3.14 GHz, 4.58 GHz, and 6.33 GHz are generated on the both side of each passbands to improve the band to band rejection. Table 1 presents a performance comparison of the proposed BPF with some other quad-band BPFs. After comparison, it is found that the proposed quad-band BPF has completely covered the bandwidths of four operating bands, good characteristics and compact size.

Table 1. Comparison between the fabricated BPF and some other quad-band BPFs.

	CF(GHz) / 3dB FBW(%)	Insertion Losses(dB)	Return Losses(dB)	Maximum Number of modes	Size (λ_g^2)
Ref.[6]	1.55/19.35, 2.2/9.09, 3.45/8.69, 5.3/3.77	0.5,1,2,4,2.9	10,18, 13,16	–	0.1800 λ_g^2
Ref.[8]	1.56/13, 2.42/4.3, 3.57/4, 5.23/2.9	1.1,2.5,2.5,2.8	16,12, 13,12.5	2	0.0480 λ_g^2
Ref.[9]	2.4/6.7, 3.5/7.2, 5.2/6.9, 5.8/5.3	2.0,1.9,1.9,1.96	15.5,14.5, 21,16	2	0.0400 λ_g^2
Ref.[10]	1.58/7.6, 1.81/8.3, 2.5/5.7, 2.66/3.7	1.1,1.3,1,1.2	12,12,15,13	4	0.0750 λ_g^2
Ref.[11]	2.44/4.96, 3.53/5.07, 5.18/2.32, 5.79/3.63	0.12,0.12,0.23,0.25	20,20,15,16	4	0.0319 λ_g^2
Ref.[12]	1.57/6.9, 2.45/3.4, 3.5/2.9, 5.2/4.7	0.78, 1.45, 2.3, 1.42	>12	4	0.0600 λ_g^2
Ref.[13]	1.8/22, 3.5/17, 5.8/10, 6.8/3	–	–	8	0.0270 λ_g^2
Ref.[14]	1.8/6.7, 2.45/4.2, 3.5/3.7, 5.5/14.8	1.5,1.7,2.3,1.8	>15	8	0.0285 λ_g^2
This work	1.55/4.06, 2.46/5.08, 3.52/7.95, 5.51/12.36	1.95, 1.61,1.17, 1.55	12.2,13.64,13.98,14.5	5	0.0240 λ_g^2

5. CONCLUSION

This paper presents a quad-band BPF based on a quintuple-mode SLTRR for GPS, WLAN, WiMAX, and 5G WiFi applications that features a compact size, high band to band isolation, single layer planar structure, and practical operation bands. Due to the wide bandwidth of 5G WiFi operating band, the last two resonant modes have been employed to cover it. The pseudo-interdigital structure has been used to generate four transmission zeros and to miniaturize the circuit size. The bandwidths of four passbands have been controlled by coupling among open-circuit arms of two SLTRRs. The methodology and design procedure indicates that the SLTRR can be attractive for designing different frequency responses.

REFERENCES

1. Yang, S., L. Lin, J. Chen, K. Deng, and C.-H. Liang, "Design of compact dual-band bandpass filter using dual-mode stepped-impedance stub resonators," *Electron. Lett.*, Vol. 50, No. 8, 611–613, Apr. 2014.
2. Guan, X., F. Wen, W. Fu, H. Liu, G. Li, and L. Zhu, "Dual-band bandpass filter using a single short-ended dual-mode resonator with adjustable first passband," *Progress In Electromagnetics Research C*, Vol. 37, 95–106, 2013.
3. Xu, K., Y. Zhang, D. Li, Y. Fan, J. L. Li, W. T. Joines, and Q. H. Liu, "Novel design of a compact triple-band bandpass filter using short stub-loaded SIRs and embedded SIRs structure," *Progress In Electromagnetics Research*, Vol. 142, 309–320, 2013.
4. Zhang, X. Y., L. Gao, Z. Y. Cai, and X. L. Zhao, "Novel tri-band bandpass filter using stub-loaded short-ended resonator," *Progress In Electromagnetics Research Letters*, Vol. 40, 81–92, 2013.
5. Sun, S. J., T. Su, K. Deng, B. Wu, and C. H. Liang, "Compact microstrip dual-band bandpass filter using a novel stub loaded quad-mode resonator," *IEEE Microw. Wirel. Compon. Lett.*, Vol. 23, No. 9, 465–468, Sep. 2013.
6. Cui, C. and Y. Liu, "Quad-band bandpass filter design by embedding dual-band bandpass filter with dual-mode notch elements," *Electron. Lett.*, Vol. 50, No. 23, 1719–1720, Nov. 2014.
7. Cheng, C. M. and C. F. Yang, "Develop quad-band (1.57/2.45/3.5/5.2 GHz) bandpass filters on the ceramic substrate," *IEEE Microw. Wirel. Compon. Lett.*, Vol. 20, No. 5, 268–270, 2010.
8. Yang, R.-Y., "Design and fabrication of a quad-band bandpass filter using multi-layered SIR structure," *Progress In Electromagnetics Research*, Vol. 114, 457–468, 2011.
9. Yan, T., X.-H. Tang, and J. Wang, "A novel quad-band bandpass filter using short stub loaded E-shaped resonators," *IEEE Microw. Wirel. Compon. Lett.*, Vol. 25, No. 8, 508–510, Aug. 2015.
10. Wu, B., F. Qiu, and L. Lin, "Quad-band filter with high skirt selectivity using stub-loaded nested dual-open loop resonators," *Electron. Lett.*, Vol. 51, No. 2, 166–168, Jan. 2015.
11. Liu, H., B. Ren, X. Guan, P. Wen, and Y. Wang, "Quad-band high-temperature superconducting bandpass filter using quadruple-mode square ring loaded resonator," *IEEE Trans. Microw. Theory Tech.*, Vol. 62, No. 12, 2931–294, Dec. 2014.
12. Wei, F., Q. L. Huang, X. H. Wang, W. T. Li, and X. W. Shi, "Compact step-impedance ring resonator for quad-band band-pass filter," *Progress In Electromagnetics Research Letters*, Vol. 41, 105–112, 2013.
13. Xiao, M., X. Li, and G. Sun, "Quad-band bandpass filter based on single stepped-impedance ring resonator," *Electron. Lett.*, Vol. 52, No. 10, 848–849, May 2016.
14. Zhang, Y., L. Gao, and X. Y. Zhang, "Compact quad-band bandpass filter for DCS/WLAN/WiMAX/5G Wi-Fi application," *IEEE Microw. Wirel. Compon. Lett.*, Vol. 25, No. 10, 645–647, May 2015.
15. Pozar, D. M., *Microwave Engineering*, 3rd Edition, Ch. 2, 49–90, Wiley, 2005.
16. Hong, J.-S. and M.-J. Lancaster, "Development of new microstrip pseudo-interdigital bandpass filter," *IEEE Microw. Guide. Wave Lett.*, Vol. 5, No. 8, 261–263, 1995.